AIMS Geosciences, 9(3): 513–527.
DOI: 10.3934/geosci.2023028
Received: 11 April 2023
Revised: 21 June 2023
Accepted: 27 June 2023
Published: 17 July 2023

http://www.aimspress.com/journal/geosciences

Research article

Minimizing the displacement of integrated system of wind and tidal turbines based on the soil types under cyclic loads

Navid Majdi Nasab[1,*] and Alan Wang[2]

[1] Mechanical Engineering Department, School of Engineering, Manukau Institute of Technology, 2023 Auckland, New Zealand.
[2] Auckland Bioengineering Institute, University of Auckland, New Zealand.

*** Correspondence:** Email: navid.nasab@manukau.ac.nz; Tel: 642102975454.

Abstract: Hybrid offshore platforms are complex structures that need to tolerate cyclic loads. These loads occur when the turbine is working between cut-in and cut-out speeds and depend on the turbine's rotational speeds. However, selecting a proper soil for the structure to be secured in is very important for the stability of the hybrid system. This study aimed to calculate the displacement of an integrated offshore structure capable of supporting a hybrid assembly of one wind plus two tidal turbines under cyclic loads. The monopile has been found to be a suitable foundation type, as the most inexpensive solution in water depths less than 30 meters, for integrating both types of turbines. The deflection of the structure was compared for different types of soil with finite element analysis. Several simulations were conducted using OPTUM G3 software for calculating the stability of each type of soil in the rotational speed range of turbines. The results enable determining the amount of deflection for each soil type. The displacement range for soft clay is 0.0052 to 0.0098 m, and displacement is between 0.007 and 0.0158 m for medium sand. The minimum displacement of firm clay, which is 0.0115 meters at 5 rpm, is higher than all minima of other soil types. Thus, soft clay and medium sand show more stability, and firm clay is less stable in the rotational speed range of the turbines.

Keywords: wind; friction angle; tidal; deflection; tilt

1. Introduction

The pursuit of renewable energy worldwide has been driven by the increasing demand for electricity and concerns about global warming caused by burning fossil fuels [1]. Offshore energy sources such as wind, sea currents and waves have gained significant attention as means of harnessing renewable energy [2].

Despite the sustainability benefits of offshore wind generation compared to onshore wind, the cost of electricity from offshore wind remains high [3,4]. The generation of tidal energy is also expensive [5]. This obstacle makes investment in tidal turbines difficult, as harsh water currents decrease the design life; and at deep-sea levels, the foundation design is complicated [6]. To address these challenges and increase power generation, a cost-effective approach involves using the same foundation for both wind and tidal turbines, tapping into two different energy sources simultaneously [7]. However, if a support structure is not correctly designed for offshore conditions, failure will be disastrous, and the structure will be costly to replace. For this reason, foundations are an essential design consideration. Several factors, including weather conditions, seabed geology, installation requirements and compliance with environmental regulations, must be considered when choosing and designing a foundation for a specific site [8].

Among various types of foundations, the monopile foundation has dominated the market due to its simplicity and cost-effectiveness [9]. However, before designing a foundation, it is essential to establish the soil profile associated with structure. Deformation is influenced by changes in effective stress, and the strength of the soil is proportional to the effective stress [10]. Hence, it is necessary to perform soil analysis under cyclic loads to determine maximum stability of foundation in the complex ocean environments.

The loads exerted on offshore structures can be static, resulting from the weight of the components, or cyclic/dynamic due to wind, wave, rotor frequency (1P) and blade-passing frequency (2P/3P) loads [11]. Considering static and cyclic loads in structural design, the concept of a hybrid pile foundation has emerged and been investigated in recent years [12]. A hybrid pile foundation combines a traditional monopile with a shallow foundation, aiming to leverage the vertical load-bearing advantages of a monopile while benefiting from additional horizontal and moment resistance provided by the shallow foundation [13].

Several types of hybrid pile foundations have been extensively studied, including finned (or winged) pile foundations [14], pile-footing foundations [15], pile-bucket (skirt) foundations [16] and hybrids derived from these three types [17]. These hybrid foundations have been widely examined and acknowledged for their superior resistance to static lateral loads and overturning moments, laying a strong foundation for studying their cyclic response. For example, Peng et al. conducted 1 g tests comparing the lateral displacement accumulation of monopile and finned piles after 10,000 load cycles, demonstrating that fins can reduce pile displacement by at least 50% [14]. However, the benefits of fins were not further felt as the fin size exceeded half the pile length. Similar comparisons have been made by Bienen et al. through centrifuge tests, showing that finned piles exhibit stiffer initial load responses and lower pile head deflections compared to monopiles [18].

Anastasopoulos and Theofilou conducted a 3D finite element analysis (FEA) to examine the lateral response of pile-footing foundations, with a specific focus on their performance under environmental

and seismic loading. The numerical results revealed that the long-term stability of the foundation would be compromised by the combination of seismic loads and cyclic environmental loads [19]. Additionally, Wang et al. performed centrifuge tests on pile-footing foundations in clay, indicating a stronger resistance to cyclic loading for hybrid piles. However, the tests were limited to only 10 load cycles [13].

Based on the preceding information, the current research primarily emphasizes the static bearing characteristics of hybrid pile foundations, with relatively less focus on their cyclic lateral response. Yet, during the operational lifespan of hybrid turbines, the supporting foundation will experience millions of load cycles due to blade rotation. Consequently, there is a lack of understanding regarding the long-term interaction between hybrid foundations and the surrounding soil.

This study presents a finite element approach to investigate the cyclic lateral responses of monopile and hybrid pile foundations, as well as their impacts on the surrounding soil. The pile and hybrid foundations are simulated as continuous materials, while the soil foundation is represented by discrete particles. First, the rotor frequency loads and their corresponding bending moments within the rotational speed range are introduced, followed by a detailed explanation of the modeling process. Subsequently, the simulation results are presented, focusing on the cyclic loads of the pile foundations and the migration patterns of different soil types. Finally, the stress development of the soil mass surrounding the pile foundation is analyzed to identify the soil type with lowest displacement.

2. Cyclic loads

The cyclic or dynamic loads affecting wind turbines arise from various sources, including wind, wave, rotor frequency (1P) and blade-passing frequency (2P/3P) loads [11].

These primary cyclic and dynamic loads can be categorized as follows:

(a) Wind load: Generated by the wind's force on the blades and tower, wind load creates cyclic or dynamic lateral forces at the hub level. The magnitude of these forces depends on the turbulence of the wind at that specific location and the operational characteristics of the turbine.

(b) Wave load: Caused by waves colliding with the substructure, wave load varies based on factors such as wave height, period and water depth.

For example, in a 3 MW wind turbine with a natural frequency of 0.3 Hz, any load with a frequency higher than 0.06 Hz is considered dynamic. Consequently, a wave loading frequency of 0.1 Hz would be classified as dynamic.

(c) 1P load: Originating from the vibration of the hub due to rotor mass and aerodynamic imbalances, the 1P load applies lateral forces and overturning moments. This load has a frequency equivalent to the rotational frequency of the rotor and is known as 1P loading. Since most industrial wind turbines are variable-speed machines, the 1P load encompasses a frequency band between the lowest and highest RPMs.

(d) Blade-passing load (2P/3P): Caused by tower vibrations resulting from blade shadowing effects, the blade-passing load has a frequency equivalent to three times the rotational frequency of the turbine (3P) for three-bladed wind turbines or two times the rotational frequency (2P) for two-bladed turbines. When turbine blades pass in front of the tower, the temporary shadowing effect reduces the thrust on the tower, leading to differential loads on the tower. Figure 1 illustrates the shadowing effect caused by two different blade configurations [20].

To guarantee the safe functioning of wind turbines throughout their lifespan of 20–30 years, it is crucial to estimate the initial dimensions of the foundation piles according to specific codes. These codes include the IEC codes (IEC 2005; IEC 2019) [21, 22] and the DNV code DNV 2014 [23]. These codes outline numerous load cases that may need to be analyzed. However, it is important to note that not all of these cases are equally significant or applicable to offshore foundation design.

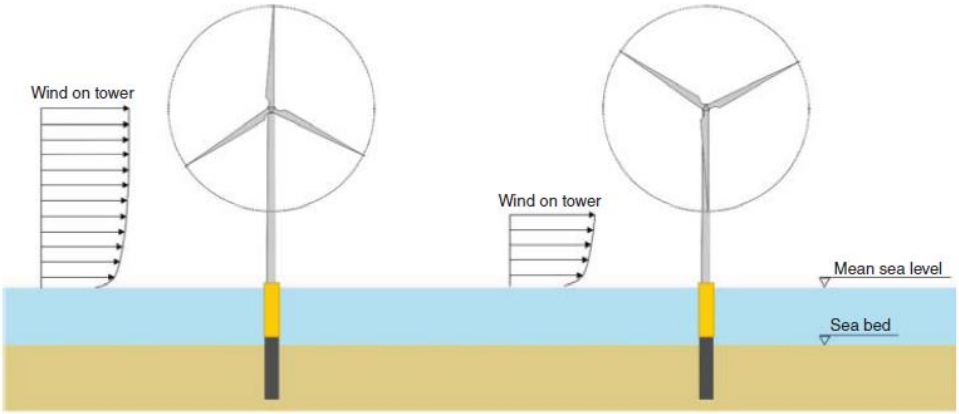

Figure 1. Explanation of 3P loading [20].

3. Methods

The monopile has emerged as a favorable choice for foundations due to its cost-effectiveness and widespread implementation in wind farm projects. It offers several advantages, including the ability to be driven into the seabed, direct connection to the tower, simplicity in structure and its established usage in wind farm projects [24]. In terms of integrating wind and tidal turbines, the monopile provides a suitable foundation type. Figure 2 illustrates the offshore structure's capability to support a hybrid arrangement consisting of one wind turbine and two tidal turbines.

Design criteria specific to the wind turbine are presented in Table 1.

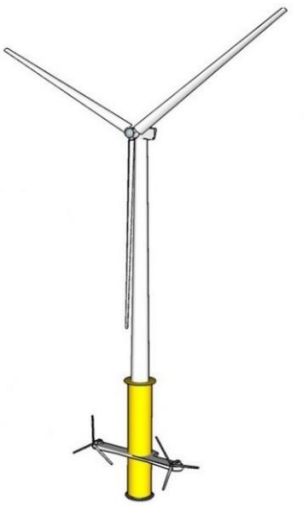

Figure 2. Schematic of a hybrid system consisting of wind and tidal turbines [25].

Table 1. General information of wind turbine, Siemens SWT-3.6-107 Offshore 3.6 MW, for the hybrid system [6,20,24,26].

Parameter	Symbol	Value	Unit
Turbine power	P	3.6	MW
Turbine rotational speed (Cut in/out)	u_{in}/u_{out}	5−13	rpm
Operational wind speed range	V	4−25	m/s
Rated wind speed	u_R	16.5	m/s
Mass of the nacelle (NA)	m_{NA}	125	tonnes
Hub height from mean sea level	H	87	m
Density of tower, monopile and TP-S355 steel	ρ	7860	kN/m^3
Tower data			
Top diameter	D_t	3	m
Bottom diameter	D_b	5	m
Weight	m_t	255	tonnes
Tower height	L_T	68	m
Wall thickness	t_T	0.027	m
Monopile data			
Monopile Young's modulus – S355 Steel	E_P	200	GPa
Soil's unit weight	γ	16	kN/m^3
Soil's internal friction	ϕ	30	°
Monopile length	L_P	60	m
Monopile diameter	D_P	6	m
Monopile thickness	t_P	0.083	m
Monopile yield stress	f_{yk}	355	MPa
Monopile weight	W_P	700	tonnes
Transition piece (TP) data			
TP Young's modulus – S355 Steel	E_{TP}	200	GPa
TP weight	W_{TP}	300	t
Transition piece internal diameter	D_{TP}	6.16	m
Transition piece thickness	t_{TP}	0.083	m
Transition piece length	L_{TP}	29	m
Grout and TP combined thickness	$t_G + t_{TP}$	0.15	m
Rotor and blade data			
Turbine rotor diameter	D	107	m
Swept area	TSA	8992	m^2
Mass of rotor + hub	m_R	100	tonnes
Rotor overhang	b	4	m
Blade root diameter	B_{root}	4	m
Blade tip chord length	B_{tip}	1	m
Blade length	L	52	m

The power curve of the Siemens SWT-3.6-107 wind turbine is depicted in Figure 3. This particular turbine represents the latest model from Siemens in the multi-MW class, featuring variable speed and pitch technology. Equation (1) presents the power equation for the wind turbine:

$$P_{wind} = \frac{3.009}{0.0008354 + e^{-0.7916V}} \tag{1}$$

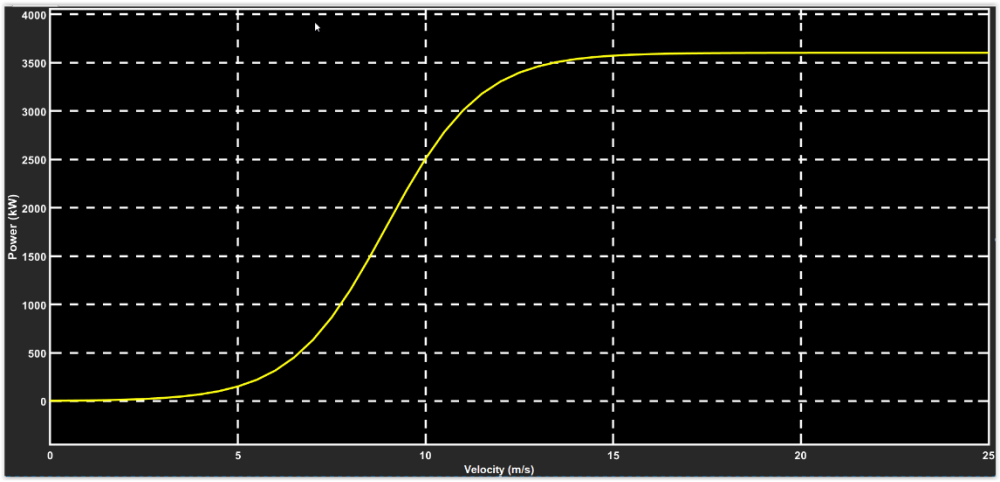

Figure 3. The power curve of the Siemens SWT-3.6MW-107m Offshore wind turbine [27].

Design criteria specific to the tidal turbine are presented in Table 2.

Table 2. General information of tidal turbine, Atlantic Resources AR 2000, for the hybrid system [20,24].

Parameter	Symbol	Value	Unit
Turbine power	P	2	MW
Turbine rotational speed (Cut in/out)	Ω	1−3.05	rpm
Operational tidal speed range	V	1−4.5	m/s
Turbine rotor diameter	D	20	m
Height from the seabed	Z_S	25	m
Rotor swept area	TSA	314	m^2
Mass of two turbines	m	300	tonnes

Figure 4 displays the power curve of the tidal turbine. This curve illustrates the power output of the turbine under varying tidal conditions. Equation (2) presents the power equation that describes the relationship between the power output of the tidal turbine and the relevant variables:

$$P_{tidal} = \frac{31.61}{0.01549 + e^{-2.156V}} \tag{2}$$

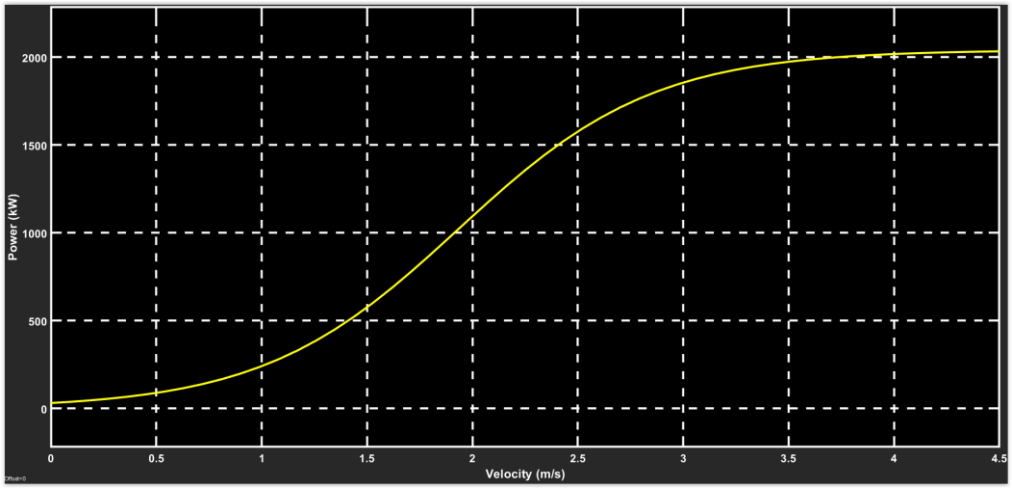

Figure 4. The power curve of the AR2000 tidal turbine [27].

The differences in the pitch of the blades cause a mass imbalance and aerodynamic imbalance in the rotor, which create cyclic loads in the structure which change with different rotational frequencies. The magnitudes of the cyclic loads depend on the mass imbalance and rotational frequency values. A straightforward approach is presented to estimate the fore-aft bending moment at the mudline resulting from the mass imbalance. However, calculating the impact of blade pitch misalignment necessitates additional input data and more advanced methodologies. The mass imbalance can be represented as an additional lumped mass on the rotor, positioned at an azimuthal angle θ from Blade I and at a distance R from the hub's center, as depicted in Figure 5. In this scenario, the imbalance is assumed to occur on Blade I (θ = 0) [28].

$$I_m = mR \tag{3}$$

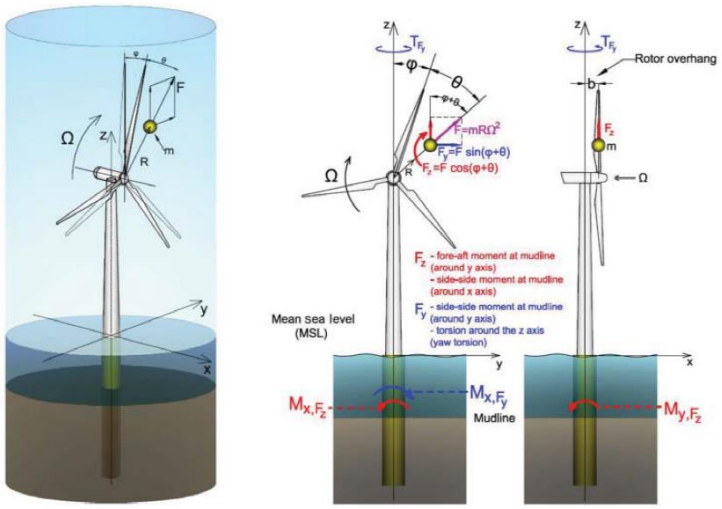

Figure 5. Model of the mass imbalance and loads exerted during operation. The fore-aft mudline bending moment caused by the wind load and waves (assumed collinear) is $M_{y,\,Fz}$ [29].

A typical value of mass imbalance for the rotor is needed to calculate I_m. From previous studies on a smaller wind turbine (2 MW Vestas V80), a mass imbalance in the range of 350 to 500 kg·m was used [30]. To estimate the imbalance value of the SWT-107-3.6 Siemens wind turbine, the assumption is made that the value is proportional to both the mass and rotor diameter. To determine the ratios for these factors, calculations are made based on the rotor specifications of the Vestas and Siemens turbines. The Vestas rotor has a mass of 37.5 tonnes and a diameter of 80 m, while the Siemens rotor has a mass of 95 tonnes and a diameter of 107 m. Using these values, the estimated imbalance value for the SWT-107-3.6 turbine is then calculated as follows:

$$I_{m,SWT107} = I_{m,V80} \cdot \frac{M_{SWT107}}{M_{V80}} \cdot \frac{D_{SWT107}}{D_{V80}} = 500 \cdot \frac{95}{37.5} \cdot \frac{107}{80} \approx 1694\ [kg \cdot m]$$

A typical value of mass imbalance for V80 is for an average operational wind turbine. To provide an upper limit estimate, one could consider a value of I_m = 2000 kg·m [20]. For finding $I_{m,AR2000}$, the same estimation can be done to reach the total I_m as below:

$$I_{m,AR2000} = I_{m,V80} \cdot \frac{M_{AR2000}}{M_{V80}} \cdot \frac{D_{AR2000}}{D_{V80}} = 500 \cdot \frac{30}{37.5} \cdot \frac{20}{80} = 100\ [kg \cdot m]$$

$$I_m = I_{SWT107} \cdot + 2I_{m,AR2000} = 2000 + 2 \times 100 = 2200\ [kg \cdot m]$$

The centrifugal force at any given time can be computed using the centrifugal acceleration formula $a = R\,\Omega^2$ where Ω represents the angular frequency, and $f = \Omega/(2\pi)$ denotes the rotational frequency. The lever arm associated with the centrifugal force F_{cf}, denoted as the rotor overhang b (as illustrated in Figure 5), is utilized to express the bending moment:

$$F_x = F_{cf} = 1P = ma = mR\,\Omega^2 = I_m\,\Omega^2 = 4\pi^2 I_m f^2 \quad (4)$$

$$M_y = M_{1P} = F_x.b \quad (5)$$

where the distance between the axis of the tower and the center of the hub (i.e., the rotor overhang) is b = 4 m.

In Figure 6, the rotational frequencies for a three-bladed Siemens 3.6 MW wind turbine are illustrated. It has a rotational operating range of 5–13 RPM. The lowest rotational speed is 5 RPM, equivalent to a frequency of 0.083 Hz (5 RPM = 5 × 1/60 = 0.083 Hz), while the rated speed is 13 RPM, equivalent to a frequency of 0.216 Hz.

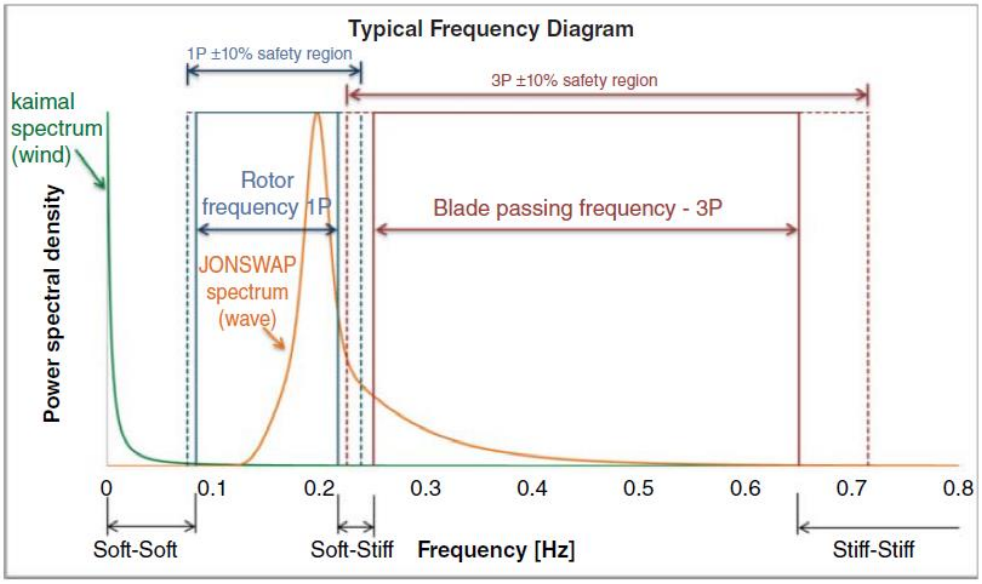

Figure 6. Frequency diagram for Siemens SWT-107-3.6 offshore wind turbine with an operating rotational wind speed range between 5 and 13 rpm [20].

1P and M_{1P} values are calculated as summarized in Table 3.

Table 3. 1P and M_{1P} in the rotational speed range.

f (rpm)	1P (N)	M_{1P} (Nm)
5	598.33	2393.308
6	868.525	3158.273
7	1182.06	4298.41
8	1476.49	5369.064
9	1954.18	7106.1
10	2412.56	8527.33
11	2919.2	10614.95
12	3474.1	12633.1
13	4052.19	14735.24

4. Results

For the present analysis, an advanced approach involving methods such as finite element analysis, discrete elements or finite differences is utilized. Figure 5 illustrates a comprehensive model of the problem, offering the advantage of incorporating complex soil behavior. To ensure accurate predictions of long-term performance, it is crucial to employ a suitable constitutive model capable of replicating realistic soil behavior under cyclic or dynamic loading conditions. While simple elastoplastic models like the Mohr-Coulomb model (based on a single yield surface without hardening), the Cam-Clay model (based on isotropic hardening) and Lade's model (based on two yield surfaces—

isotropic and deviatoric loading) prove effective and efficient in simulating soil behavior under monotonic conditions, they are not suitable for modeling cyclic loading. In such models, plastic deformations typically occur beyond a certain loading threshold, often surpassing the magnitude of the cycles. Consequently, the simulated soil behavior remains elastic below this threshold, which contradicts experimental evidence, particularly for granular materials [20]. Therefore, the OPTUM G3 model is employed, taking into account the values provided in Tables 1, 2, and 3 as depicted in Figure 7. OPTUM G3 serves to represent different soil types for the foundation and examines how the specific soil type impacts the stability of the hybrid system. Optum CE is a software package that offers fast and user-friendly tools for the design of geotechnical and concrete structures. The software is developed with a focus on providing advanced finite element analysis capabilities while ensuring accessibility for engineering practitioners, including structural engineers, contractors and building companies [26].

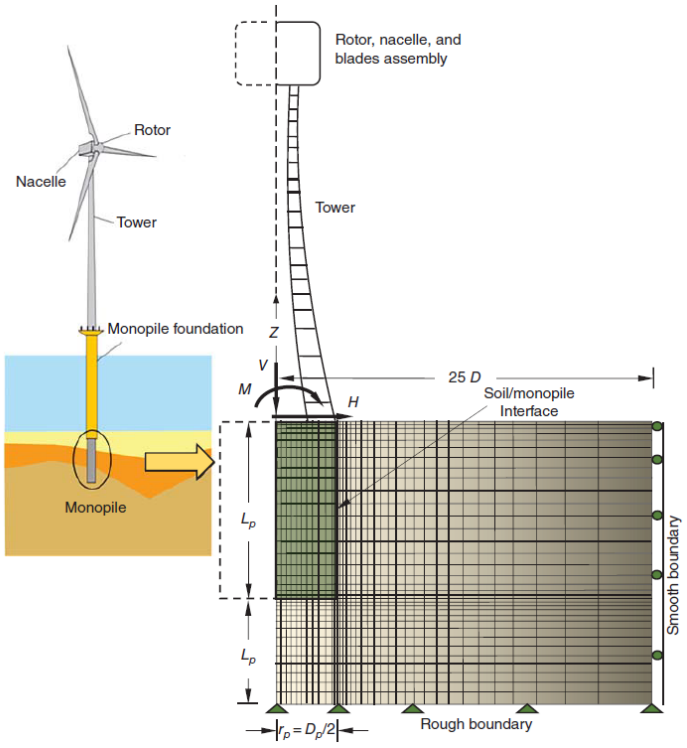

Figure 7. Finite elements of a monopile and surrounding elastic medium [20].

Table 4 shows the parameters used by OPTUM for simulations.

The unit weight of a soil mass is the ratio of the total weight of soil to the total volume of soil. The total mass of the structure after summarizing the weights of each element in Tables 1 and 2 is 1780 tonnes. Figure 8 shows how OPTUM G3 [26] is used to apply cyclic loads to the foundation.

After simulation by OPTUM, the results for different kinds of soils for different rotational speeds are represented in Figures 9 to 14.

Several simulations were conducted for loose sand, medium sand, dense sand, soft clay, firm clay and stiff clay in the rotational speed range of 5 to 13 rpm. After meshing of the model, the software calculates the displacement of the foundation. The geometry after meshing and displacement for Loose Sand-MC at 5 rpm is shown in Figure 9 as an example.

Table 4. Geotechnical parameters used by OPTUM software for simulations.

Item	Loose Sand-MC	Medium Sand-MC	Dense Sand-MC	Soft Clay-MC	Firm Clay-MC	Stiff Clay-MC
Cohesion c (kPa)	0	0	0	5	10	20
Friction angle ϕ (°)	30	35	40	18	20	22
Soil Unit Weight γ (kN/m^3)	16	18	20	19	20	21

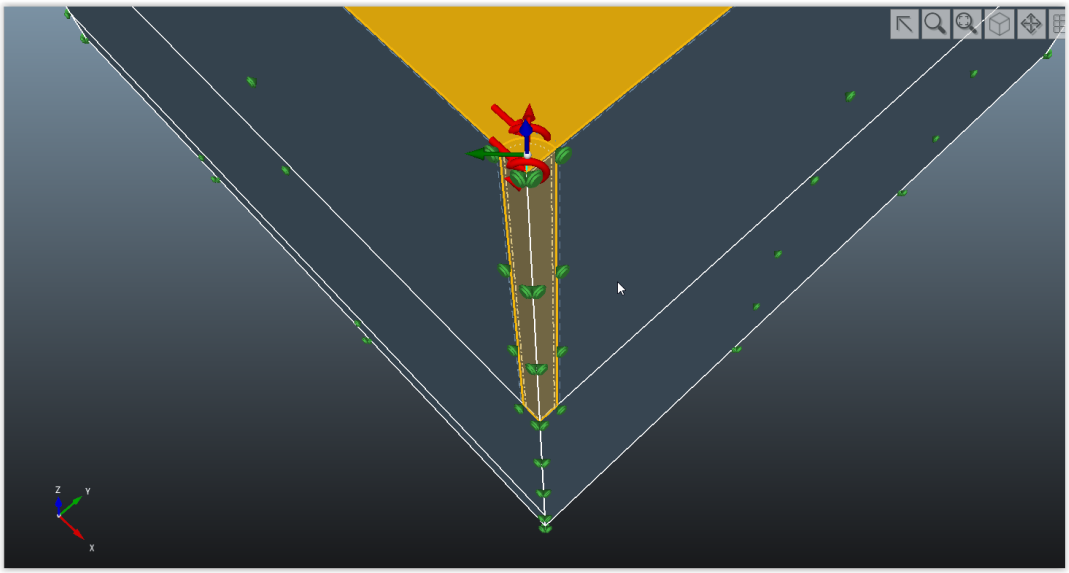

Figure 8. Applying cyclic loads to the structure using OPTUM.

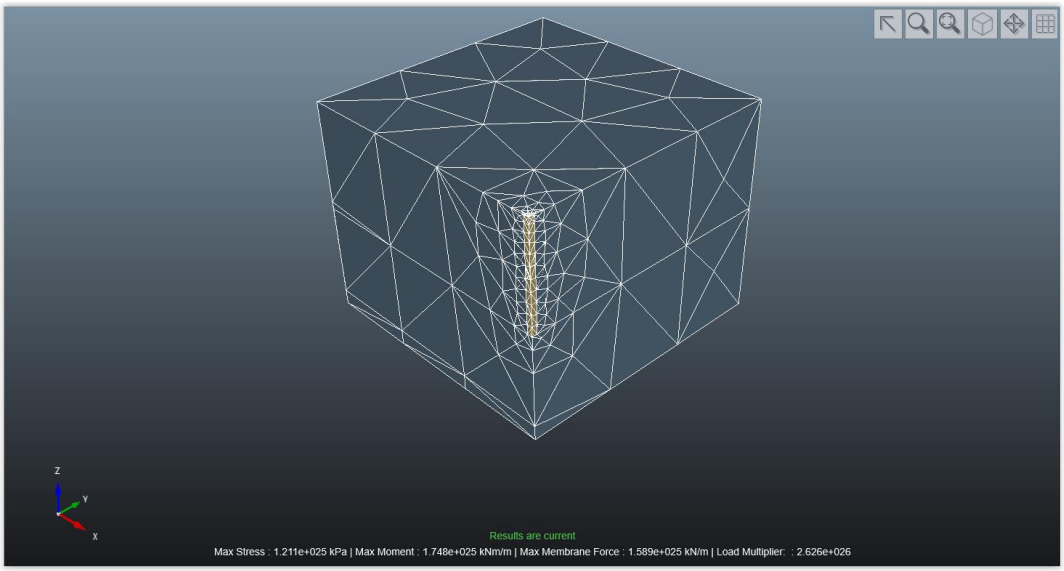

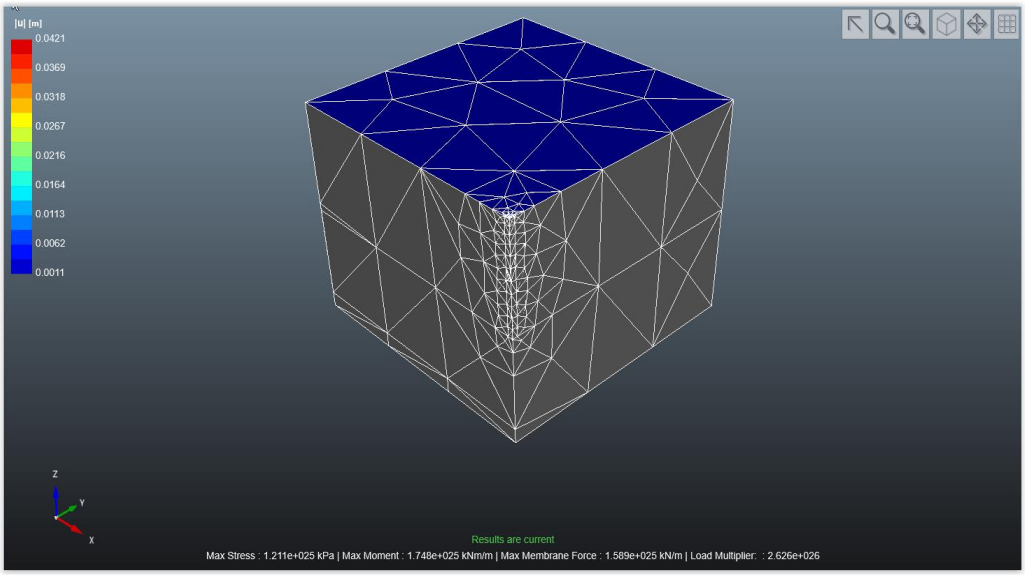

Figure 9. The geometry after meshing (top) and displacement (bottom) for Loose Sand-MC at f = 5 rpm.

Figure 10 summarizes the results of displacement for soils in the operating rotational range.

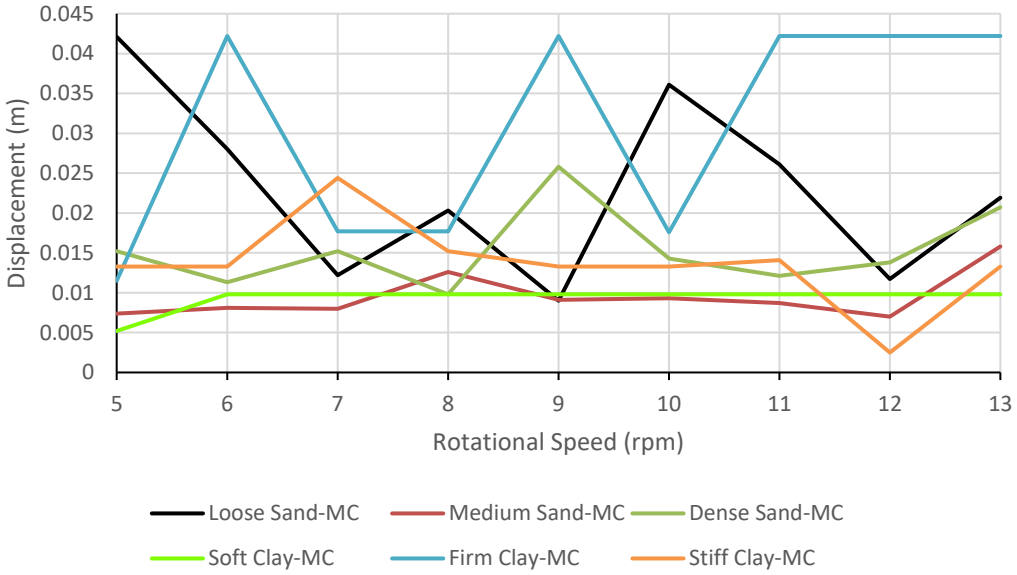

Figure 10. The displacement of hybrid wind and tidal turbines structure within operating rotational range 5-13 rpm for different soils.

5. Conclusions

The acting loads are transferred to the foundation. They can be static depending on the total weight of structure. They were calculated and analyzed with OPTUM G3 software for dynamic (cyclic) combined wind and wave loads.

The acceptability of foundation design depends on the stability of the structure under loads. From applying cyclic loads for different soils, the following can be understood:

- The maximum displacement can be seen for firm clay with 0.0422 meters for 6, 9, 11, 12 and 13 rpm. Even minimum displacement of firm clay, which is 0.0115 meters for 5 rpm, is higher than all minima of other soil types. So, clearly, firm clay is not a suitable soil considering this differential range.
- While minimum displacement occurs at 12 rpm for stiff clay soil (0.0025 m), the displacement values for soft clay and medium sand are less in the operating rotational range compared to others. The displacement range for soft clay is between 0.0052 and 0.0098 m, and it is between 0.007 to 0.0158 m for medium sand.
- The displacement of soft clay starts at 0.0052 m at 5 rpm, and then it works constantly at 0.0098 m for other rpms. This value is much less than displacements happening for firm clay, dense sand and loose sand soils. The only exceptions are for dense sand at 8 rpm (0.0098 m) and loose sand at 9 rpm (0.009 m). Having a stable displacement can be an advantage for using soft clay.

The future work in this aspect can be estimating the the displacement of structures for different soils for vertical (deadweight) loads.

Data availability statement

Data is available on request from the authors.

Use of AI tools declaration

The authors declare they have not used Artificial Intelligence (AI) tools in the creation of this article.

Conflict of interest

The authors declare no conflict of interest.

References

1. Nasab NM, Kilby J, Bakhtiaryfard L (2020) Wind Power Potential Assessment for Three Locations in New Zealand. *Chem Eng Trans* 81: 73–78. https://doi.org/10.3303/CET2081013
2. Li L, Gao Y, Yuan ZM, et al. (2018) Dynamic response and power production of a floating integrated wind, wave and tidal energy system. *Renewable Energy* 116: 412–422. https://doi.org/10.1016/j.renene.2017.09.080
3. Noori M, Kucukvar M, Tatari O (2015) Economic input–output based sustainability analysis of onshore and offshore wind energy systems. *Int J Green Energy* 12: 939–948. https://doi.org/10.1080/15435075.2014.890103
4. Heptonstall P, Gross R, Greenacre P, et al. (2012) The cost of offshore wind: Understanding the past and projecting the future. *Energy Policy* 41: 815–821. https://doi.org/10.1016/j.enpol.2011.11.050

5. Nasab NM, Kilby J (2021) Feasibility Study: Effect of Tidal Turbines Cut-in Speed for Power Generation in New Zealand. *Chem Eng Trans* 88: 13–18. https://doi.org/10.3303/CET2188002
6. Majdi Nasab N, Islam MR, Muttaqi K, et al. (2021) Optimization of a Grid-Connected Microgrid Using Tidal and Wind Energy in Cook Strait. *Fluids* 6: 426. https://doi.org/10.3390/fluids6120426
7. Gruszczynski A (2017) Hybrid Offshore Wind and Tidal. Available from: http://www.esru.strath.ac.uk/EandE/Web_sites/16-17/WindAndTidal/index.html.
8. Nasab NM, Kilby J, Bakhtiaryfard L (2022) Integration of wind and tidal turbines using spar buoy floating foundations. *AIMS Energy* 10: 1165–1189. https://doi.org/10.3934/energy.2022055
9. Zhang Y, Liu H, Wu WB, et al. (2021) Interaction model for torsional dynamic response of thin-wall pipe piles embedded in both vertically and radially inhomogeneous soil. *Int J Geomech* 21: 04021185. https://doi.org/10.1061/(ASCE)GM.1943-5622.000216
10. Fellenius B (2017) *Basics of foundation design*, Lulu. com.
11. Majdi Nasab N (2022) A Feasibility Study of a Hybrid Power Generation System Using Offshore-wind Turbine and Tidal Turbine. Auckland University of Technology.
12. Chen D, Gao P, Hunag SS, et al. (2020) Static and dynamic loading behavior of a hybrid foundation for offshore wind turbines. *Mar Struct* 71: 102727. https://doi.org/10.1016/j.marstruc.2020.102727
13. Wang X, Zeng XW, Li XY, et al. (2019) Investigation on offshore wind turbine with an innovative hybrid monopile foundation: An experimental based study. *Renewable Energy* 132: 129–141. https://doi.org/10.1016/j.renene.2018.07.127
14. Peng J, Clarke B, Rouainia M (2011) Increasing the resistance of piles subject to cyclic lateral loading. *J Geotech Geoenviron Eng* 137: 977–982. https://doi.org/10.1061/(ASCE)GT.1943-5606.0000504
15. Lehane B, Pedram B, Doherty JA, et al. (2014) Improved performance of monopiles when combined with footings for tower foundations in sand. *J Geotech Geoenviron Eng* 140: 04014027. https://doi.org/10.1061/(ASCE)GT.1943-5606.0001109
16. Haiderali A, Madabhushi G (2016) Improving the lateral capacity of monopiles in submarine clay. *Proc Inst Civil Engineers-Ground Improv* 169: 239–252. https://doi.org/10.1680/jgrim.14.00039
17. Wang X, Zeng XW, Li XY, et al. (2020) Liquefaction characteristics of offshore wind turbine with hybrid monopile foundation via centrifuge modelling. *Renewable Energy* 145: 2358–2372. https://doi.org/10.1016/j.renene.2019.07.106
18. Bienen B, Dührkop J, Grabe J, et al. (2012) Response of piles with wings to monotonic and cyclic lateral loading in sand. *J Geotech Geoenviron Eng* 138: 364–375. https://doi.org/10.1061/(ASCE)GT.1943-5606.000059
19. Anastasopoulos I, Theofilou M (2016) Hybrid foundation for offshore wind turbines: Environmental and seismic loading. *Soil Dyn Earthq Eng* 80: 192–209. https://doi.org/10.1016/j.soildyn.2015.10.015
20. Bhattacharya S (2019) *Design of foundations for offshore wind turbines*, Wiley Online Library.
21. IEC 61400. Available from: https://en.wikipedia.org/wiki/IEC_61400.
22. BS EN IEC 61400-3-1: 2019 Wind energy generation systems. Design requirements for fixed offshore wind turbines. BSI Standards Limited. Available from: https://webstore.iec.ch/publication/29360.

23. DNV G (2014) *Environmental conditions and environmental loads*. Recommend Practice DNV-RP-C205.
24. Karimirad M (2014) *Offshore energy structures: for wind power, wave energy and hybrid marine platforms*. Springer.
25. Nasab NM, Kilby J, Bakhtiaryfard L (2022) Analysis and Design of Monopile Foundations for Offshore Wind and Tidal Turbine Structures. *Water* 14: 3555. https://doi.org/10.3390/w14213555
26. OPTUM CE. Available from: https://optumce.com/.
27. Nasab NM, Kilby J, Bakhtiaryfard L (2020) The Potential for Integration of Wind and Tidal Power in New Zealand. *Sustainability* 12: 1–21. https://doi.org/10.3390/su12051807
28. Bowles L (1996) *Foundation analysis and design*, McGraw-hill.
29. Arany L, Bhattacharya S, Adhikari S, et al. (2015) An analytical model to predict the natural frequency of offshore wind turbines on three-spring flexible foundations using two different beam models. *Soil Dyn Earthq Eng* 74: 40–45. https://doi.org/10.1016/j.soildyn.2015.03.007
30. Augustesen AH, Brødbæk KT, Møller M, et al. (2009) Numerical modelling of large-diameter steel piles at Horns Rev. *Proceedings of the Twelfth International Conference on Civil, Structural and Environmental Engineering Computing*, Civil-Comp Press.

AIMS Press